DOI: 10.2507/33rd.daaam.proceedings.xxx

IDENTIFICATION OF THE COW'S NIPPLES USING A 3D CAMERA WITH TOF TECHNOLOGY

Denis Shilin, Pavel Ganin, Dmitry Shestov, Andrey Novikov, Nikolay Grebenshchikov, Dmitry Pavkin, Semyon Ruzin & Sergey Yurochka

This Publication has to be referred as: Shilin, D[enis]; Shestov, D[mitry]; Ganin, P[avel]; Novikov, A[ndrey]; Grebenshchikov, N[ikolay]; Pavkin, D[mitry]; Rusin, S[emyon] & Yurochka S[ergey] (2022). Identification of the cow's nipples using a 3D camera with ToF technology, Proceedings of the 33rd DAAAM International Symposium, pp.xxxx-xxxx, B. Katalinic (Ed.), Published by DAAAM International, ISBN 978-3-902734-xx-x, ISSN 1726-9679, Vienna, Austria
DOI: 10.2507/33rd.daaam.proceedings.xxx

Abstract
The paper considers the use of a 3D camera with ToF technology to identify biological images in the form of a cow's udder. An algorithm has been developed that is autonomously able to recognize the desired point clouds related to individual nipples. The algorithm has been tested and can be used as a basis for further search for positioning points of the working bodies of the milking manipulator.

Keywords: Data analysis; Milking machine; 3D ToF Camera; Udder of a cow; Point cloud.

1. Introduction

A three-dimensional time-of-flight camera or 3D ToF is a type of non-scanning lidar (a device for detecting, identifying and determining range using light), which uses powerful optical pulses of several nanosecond durations to capture depth information (usually, at short distances) within the region of interest. Time-of-Flight cameras are most often used as follows: navigation in a confined space, gesture recognition, scanning objects, tracking objects, measuring volumes, monitoring the target area, fast accurate indication of the distance to the target, augmented reality, evaluation of the size and shape of objects [1], [2], [3], [4], [5], [6], [7], [8], [9]. So, the first smartphone with a ToF camera was the iPhone X, released in the fall of 2017. It is a key element of the FaceID system that scans the user's face. In 2015, with the help of a drone and a camera with ToF technology, a three-dimensional image of the statue of Christ the Savior in Brazil was successfully created. Prior to this, an exact model of this statue did not exist. ToF technology is used not only on drones and telephones, but also in various areas, such as: logistics, surveillance and security, robotics, medicine, games, photos, film production, auto industry, archeology, environmental projects, and farm automation [10]. Sensors such as lidars (used in Lely milking robots), lidar flashes, 360-degree 3D lidars and TOF cameras (used in Lely, GEA, DeLaval milking robots) are built on TOF technology. The principles of TOF depth measurement are divided into pulse

modulation, CW modulation, and pseudo noise modulation. TOF are used when it is necessary to analyze the volume, shape of an object, to determine the position of an object in three-dimensional space relative to the world coordinate system. Use as a head module to control a self-propelled or self-propelled object. Choi [11] developed a navigation system for a combine harvester using pulse modulation technology. The system has been tested under static and dynamic conditions with 0.02 m and 0.07 m rms errors. Ifm [12] has developed an intelligent sensor with continuous wave modulation, where the emitter is located in a separate unit from the receiver. The sensor is specially designed for outdoor use, which does not react to interference such as sunlight, materials with various reflective effects (glare resistant). The system captures contour lines, which makes it possible to recognize up to 20 different objects at a distance of up to 35 m. In studies [13], a system was developed based on TOF technology (modulation of continuous waves), which was protected from wind and sunlight. The authors found the superiority of TOF over stereo imaging sensors, as well as low TOF resolution and small viewing angle. Studies [14] used a combination of a two-dimensional camera with TOF (continuous wave modulation) to assess apple yield. The authors were able to recognize up to 88% of apples, noting that a high percentage was provided by images from multiple angles. The remaining 12% were not identified due to the fact that they were covered with branches and leaves. Lidar systems are more often used to solve geodetic problems. Large corporations use lidars to develop self-driving cars. In studies [15] Akhloufi M.A it was found that the use of the lidar system for scanning the teat of a cow's udder is not 100% effective. In studies [16], images of maize plants were obtained using lidar. It was found that for the correct obtaining of the results, the angle of installation of the lens of the three-dimensional sensor in relation to the object under study is important. In studies [17], the authors used a three-dimensional lidar -360 ° as a navigation sensor. Factors such as reaction of cows to the presence of a robot, remote control and tracking were positively assessed. In the framework of this article, the question of using a 3D camera to detect a biological image in the form of nipples of an udder of a cow is considered. Automatic identification is necessary for automated milking of an animal.

2. Automated Milking Plants

In existing automatic milking systems of various manufacturers, including Lely, Gea Farm, DeLaval, there are drawbacks associated with alternately putting on milking cups with a long time interval, which contribute to reducing the release of oxytocin due to delays in the stimulating effect on the nipple receptors, which leads to to incomplete elimination of milk from the alveoli. Moreover, the advantage of such systems is the absence of need to search and analyze all biological objects at the same time. The relevance of this work is the development of an identification algorithm for all the nipples of a cow with the aim of further analysis and the formation of positioning points for the working bodies of the milking robot, the kinematics of which allow positioning at all desired points at the same time.

Typically, such installations consist of multi-link manipulators driven in motion by a pneumatic or electric motor. In the work of Dorokhov A., et al. the question is just being considered of choosing the kinematic model of such manipulators and the location of the drive equipment to ensure the required reachable areas of the working body [18]. The solution of the kinematics problems is considered by Gnin M.E., et al. [19]. The authors developed an algorithm for solving kinematics problems, which provides for scaling when changing the design parameters and the number of manipulator links. The search for a solution to kinematic problems is based on a neural network approach in combination with numerical refinement algorithms.

An important part of the automatic milking system for cows is the automatic nipple recognition system for the cow. This task is not effectively solved with the help of technical vision, since in this case it is necessary to know for sure the necessary threshold value for the preparation of the original image in order to detect the desired object, so Figure 1 shows the result of the preparation of the original image.

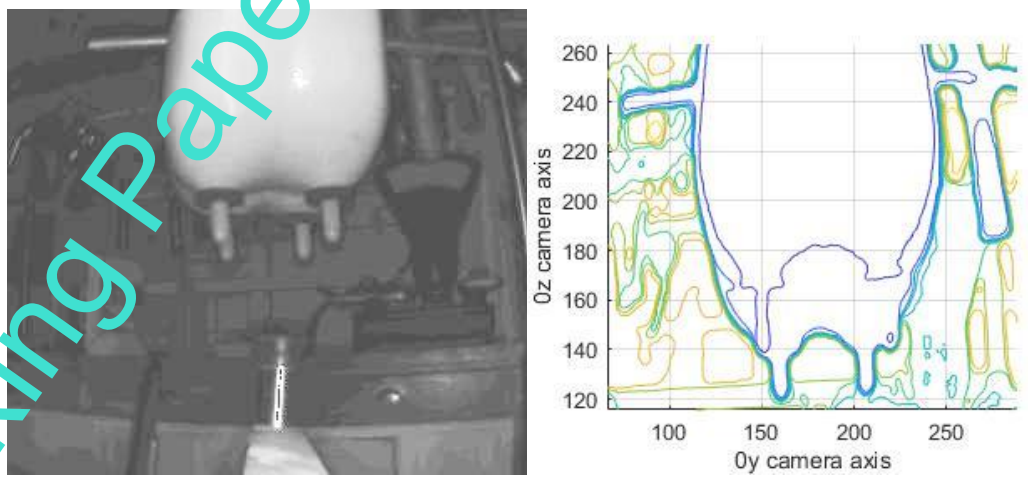

a b

Fig. 1. The result of the preparation of the original image: a) the original image, b) the binarized image with various threshold values

As you can see, when a threshold value changes in a certain range, they lead to the formation of many contours; accordingly, not knowing the exact threshold value for a particular case makes it impossible to accurately determine the coordinates of the desired object [20]. Nevertheless, there are algorithms where the aforementioned problem is solved by introducing intuitive parameters that provide a compromise between undersegmentation and excessive segmentation [21], [22] or segmentation of objects using the evaluation method core density, after which the points are divided into objects [23]. Nevertheless, when controlling robotic systems, it is recommended to use 3D ToF cameras as feedback [10].

3. Description of the experimental laboratory stand

The testing of the developed algorithms was carried out at the laboratory bench shown in Figure 2 in the 0zx plane. A plastic udder model was used as the object under study, and a 3D ToF camera was used as a camera. There are a huge number of cameras with ToF technology, their detailed comparison is presented by Deckers, N. and Peulke, R. [24]. In this work, we used IFM O3D303 capable of capturing an image in the format [264,352] in real time with a frequency of 25 Hz. The device has a working range from 0.3 m. to 8 m. And provides distance information in real time. A detailed discussion of the camera can be found in Bogaerts et al. [25]. Various techniques and techniques for processing signals from a ToF camera are disclosed in Kolb et al. [26]. Recognizing the objects in the image alone is not enough for the full functioning of the system, it is also necessary to know the location of the objects found relative to a certain reference frame. This is another reason to use an industrial camera with the ability to visually assess the distance - a 3D camera with ToF technology.

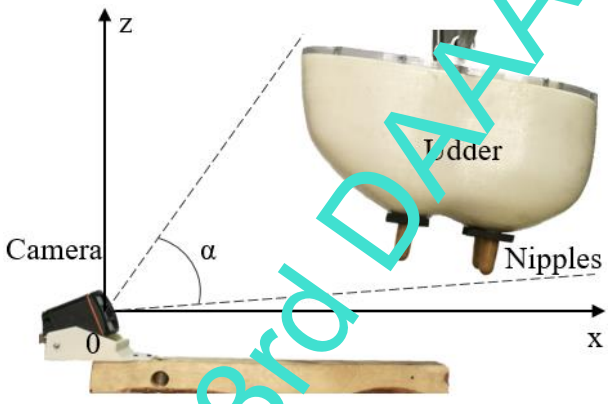

Fig. 2. The appearance of the laboratory bench in the 0zx plane

Knowing the aperture angles α (see Figure 2) and β along the axes 0x and 0y of the camera allow to build a point cloud in the space 0xyz. In order to automatically recognize biological objects in the form of nipples of the udder of a cow, it is necessary, first, to define a cloud of points of the udder itself.

4. Defining an udder point cloud

In the existing and developing milking machine robot, a 3D camera, which serves as feedback when controlling the positioning of the working bodies, is installed near the object, as shown in Figure 3. This arrangement ensures the location of the udder points in the center of the entire cloud of points, and at the closest possible distance to the camera.

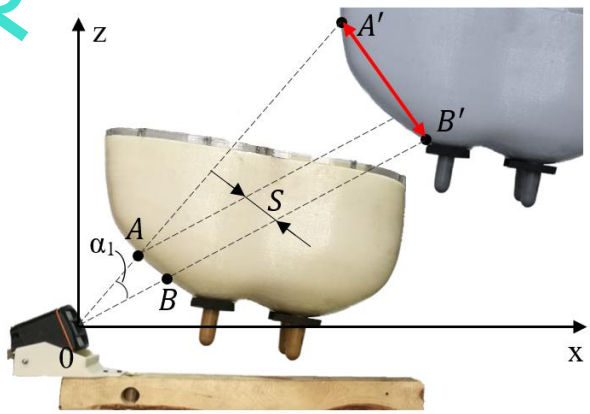

Fig. 3. The dependence of the distance between points on the location of the object on the plane 0zx

In Figure 3, points A and B are adjacent points, the distance **S** between them increases with increasing distance between the camera and the tracking object. According to the foregoing, an experimental range of values [0, **S**] was selected, which eliminated all points, the distance between which exceeded the permissible value of **S**. The range set by the operator [0, **S**] guaranteed no screening of the udder points. The distance between point A and B is calculated using the following equation:

$$\mathbf{S} = \sqrt{(\mathbf{x_A} - \mathbf{x_B})^2 + (\mathbf{y_A} - \mathbf{y_B})^2 + (\mathbf{z_A} - \mathbf{z_B})^2}, \quad (1)$$

where $(\mathbf{x_A}, \mathbf{y_A}, \mathbf{z_A})$ – coordinates of point A, m; $(\mathbf{x_B}, \mathbf{y_B}, \mathbf{z_B})$ – coordinates of point B, m.

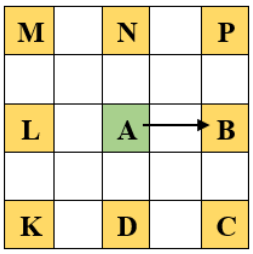

Fig. 4. The location of all adjacent points with point A

If the value of **S** is within the admissible value that is set by the operator, the entire series of points from A to B will enter the object and the verification of the point's belonging to the cloud is terminated, in this case, the cloud number that was indicated earlier at point B is assigned, or a new number is assigned (see figure 4). If the value of S is not in the acceptable range [0, **S**], then a similar verification of the distance to the points B, C, D, K, L, N, M, P follows.

Figure 5 shows an example of the work of the approach for searching point clouds. Checking points is carried out diagonally, provided that earlier the check was not carried out and not a single cloud of points was formed. For the first point, the admissible value of S was calculated to point B (see Figure 3), the second to the point D, the third to the point P, the fourth to the point L, and the fifth - the admissible value **S** was not found in all available options. Figure 5 shows that as a result of testing the algorithm, three-point clouds were found, the largest of which is marked with a red frame.

Figure 6 shows all the points that fit the specified requirement, where the purple color indicates the points that do not exceed the allowable value of S on the diagonals, blue - on the horizontal and vertical. Since the 3D camera is installed at the smallest distance to the udder, the largest point cloud (cluster of points) will be a point cloud consisting of cow udder points. Figure 7 shows in black the largest point cloud that was detected in the experiment.

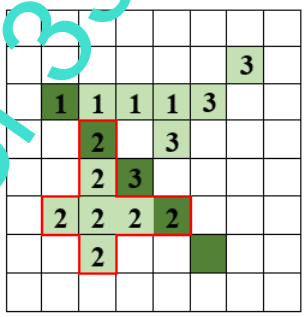

Fig. 5. An example of a point cloud search algorithm

For further analysis of the obtained cloud of the udder points of the cow, it is necessary to clarify with all the points that were not included according to the verification of permissible distances, but according to biological features probably related to this cloud of udder points. To do this, it is necessary to include in the cloud of udder points of the cow all the points from the original cloud of points that fall into the range $[\mathbf{x_{min}}, \mathbf{x_{max}}]$, $[\mathbf{y_{min}}, \mathbf{y_{max}}]$ and $[\mathbf{z_{min}}, \mathbf{z_{max}}]$, where $\mathbf{x_{min}}$, $\mathbf{y_{min}}$, $\mathbf{z_{min}}$, are the minimum values of the coordinates of the points along the x, y, and z axes, respectively, $\mathbf{x_{max}}$, $\mathbf{y_{max}}$, $\mathbf{z_{max}}$, are the maximum values of the coordinates of the points **x**, ***y***, and **z** axes, respectively. Figure 7 shows in red a refined cloud of cow udder points.

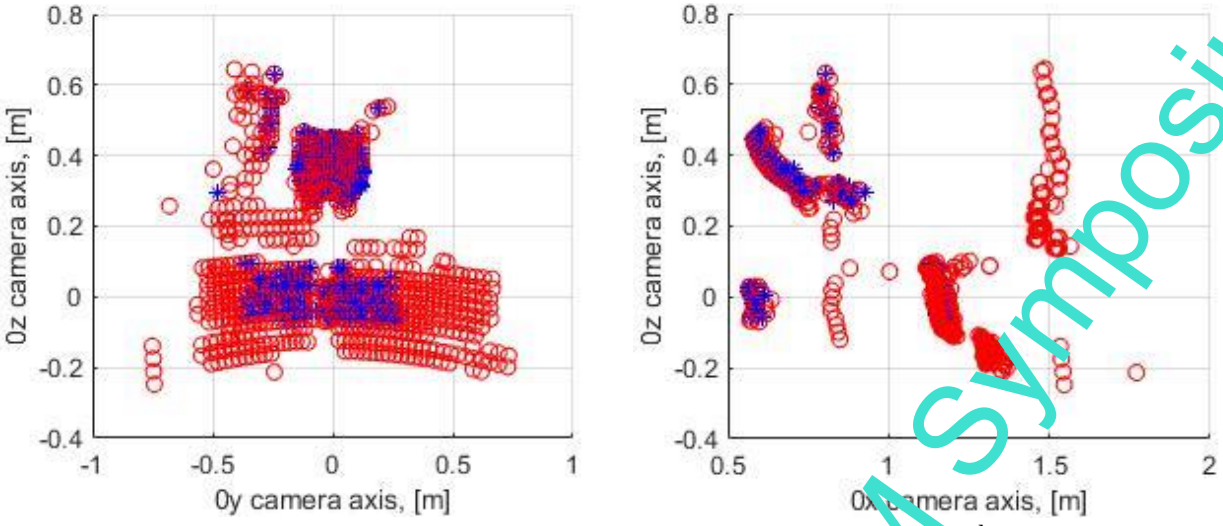

a b

Fig. 6. The cloud of points, the distance between which does not exceed S: a) a front view, b) a side view

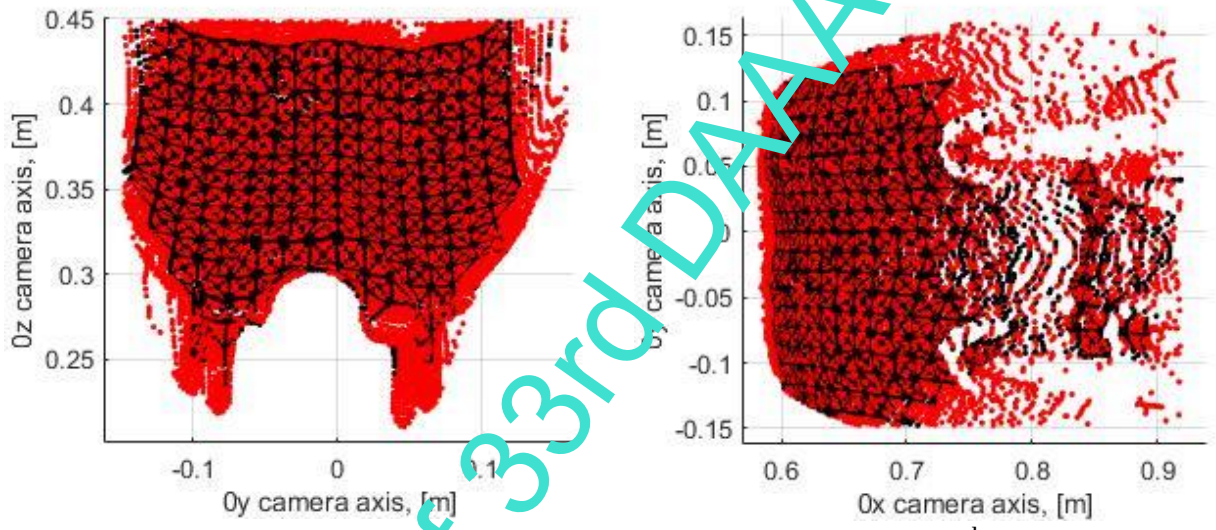

a b

Fig. 7. The cloud of udder points: a) front view, b) top view

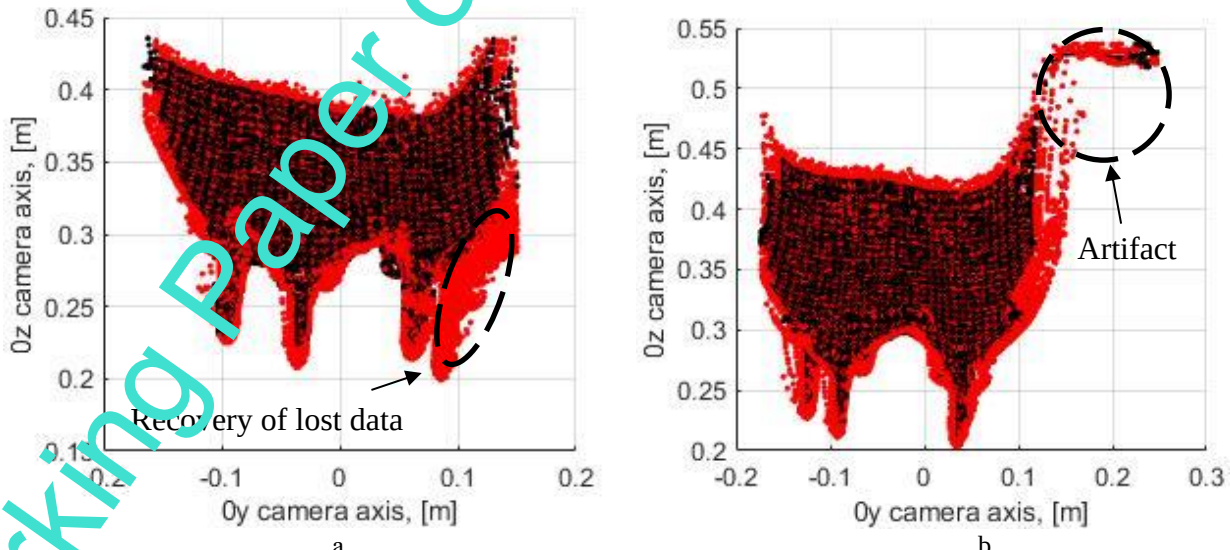

a b

Fig. 8. Positive and negative impact of refinement of the point cloud: a) restoration of lost data, b) strengthening of artifacts

The aforementioned refinement has an important merit - for example, Figure 8a shows that after identifying the largest point cloud, information about the 4 nipples did not fit into the cloud, while the rectification of this cloud made it possible to fill in the lost data. In this case, there may be cases with a negative effect (see Figure 8b), when the point cloud contains artifacts.

5. Defining cow nipple point clouds

Knowing the biological features of the structure of the cattle udder and the generalized location of the nipples on the udder, we can conclude that of all the received points of the udder cloud of the cow, those points that are located below the udder, or with the smallest coordinate along the 0z axis, are of most interest. To eliminate unnecessary points, their total number was divided into 10 identical sections along the 0z axis to calculate them and determine the section with the largest content (see Figure 9). In graphic display (see Figure 9a), it is seen that the area in the center of the image is the most massive in terms of the number of points in it. Figure 9b shows the dependence of the number of points in a section on the number of sections where you can determine the exact section with the maximum number of points. Also, this section can be determined by taking the derivative of the function that describes this dependence and equating it to zero:

$$\begin{aligned} &\mathbf{x} = -81{,}6 \cdot y^2 + 858{,}5 \cdot y - 505{,}2, \\ &\mathbf{x}' = -163{,}2 \cdot y + 858{,}5, \\ &\mathbf{x}' = 0, \\ &163{,}2 \cdot \mathbf{y} = 858{,}5, \\ &\mathbf{y} = 5{,}26 \rightarrow \mathbf{x} = -81{,}6 \cdot 5{,}26^{\,2} + 858{,}5 \cdot 5{,}26 - 505{,}2 = 1752 \text{ points.} \end{aligned} \tag{2}$$

In order to free up operational space, all data about points located outside is deleted, since they do not contain any information about the nipples.

By the identification of biological images is meant the detection of nipples and the formation of individual point clouds. In order to identify the desired objects, as in determining the cloud of the udder of a cow, the distances between the points were calculated by the equation (1). Next, a point cloud was determined, which includes the largest number of points and calculated its average location coordinates using the following equations:

$$\mathbf{x_{mid}} = \left[\sum_{i=1}^{n} \mathbf{x}\right] \Big/ \mathbf{n}, \mathbf{y_{mid}} = \left[\sum_{i=1}^{n} \mathbf{y}\right] \Big/ \mathbf{n}, \mathbf{z_{mid}} = \left[\sum_{i=1}^{n} \mathbf{z}\right] \Big/ \mathbf{n} \tag{3}$$

where $\mathbf{n}$ – the number of points in the cloud, pcs; $(\mathbf{x_{mid}}, \mathbf{y_{mid}}, \mathbf{z_{mid}})$ – coordinates of the center of this point cloud, m.

When determining the subsequent biological images, it is also necessary to compare the found coordinates of the center of the current cloud so that they do not enter the zone described by the radius R relative to the center of another cloud of points (see Figure 10):

$$(\mathbf{x} - \mathbf{x'_{mid}})^2 + (\mathbf{y} - \mathbf{y'_{mid}})^2 + (\mathbf{z} - \mathbf{z'_{mid}})^2 > \mathbf{R}^2, \tag{4}$$

where (x, y, z) - coordinates of the center of the current point cloud, m; R is the radius described zone relative to the center of another cloud of points, m; $(\mathbf{x'_{mid}}, \mathbf{y'_{mid}}, \mathbf{z'_{mid}})$ - coordinates of the center of the previous point cloud, m.

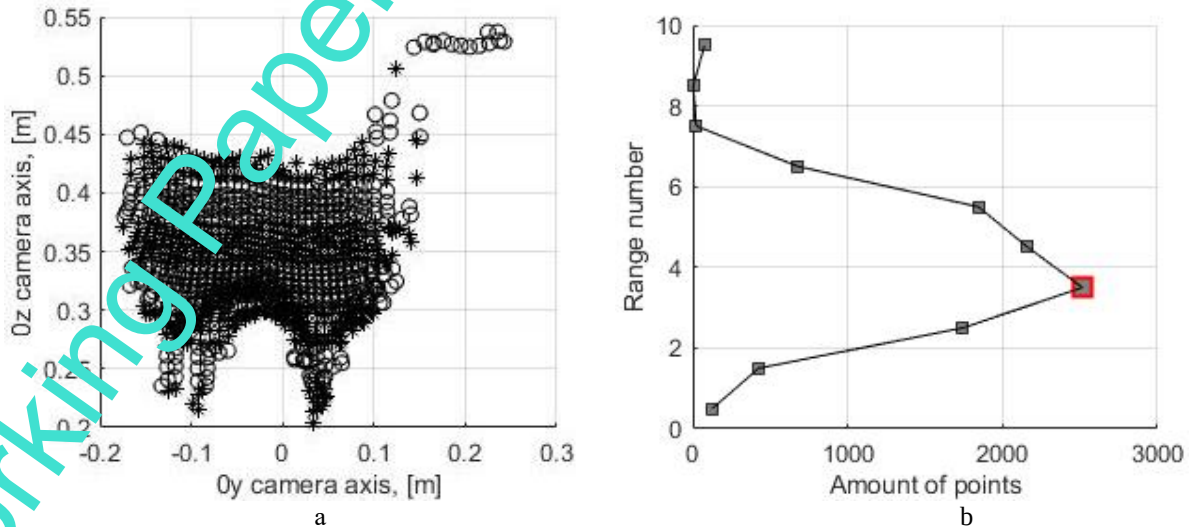

a b

Fig. 9. Search for an area with a maximum number of points: a) dividing a point cloud into equal sections, b) a graphical representation of the dependence of the considered point cloud segment on the number of points in it

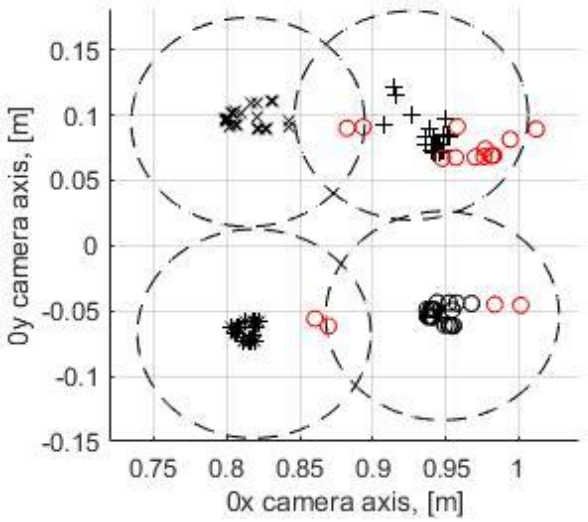

Fig. 10. Zones described around the centers of point clouds found

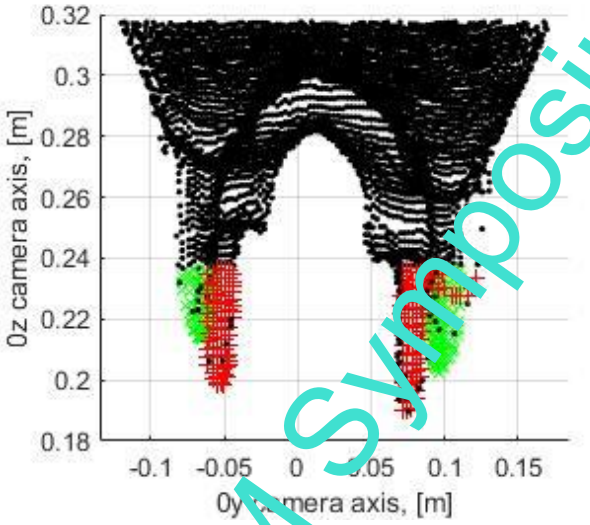

Fig. 11. Fixation of point clouds, characterizing each separately the nipple of the animal

Figure 10 shows the red points that are not included in any of the found point clouds. In Figure 11, on the 0yz plane, biological images are shown in red and green dots that satisfy the requirements of (4), and are the desired point clouds that characterize each individually nipple of the animal

As a further continuation of ongoing research, the authors propose the use of a methodology for finding the dimensions, orientation and position parameters of a parabolic ellipsoid, which was proposed by Min Dai, et al. [27]. It is assumed that this approach will determine the parameters of the elliptical paraboloid that describes the cow's nipple.

6. Conclusions

Based on the work done, the following conclusions can be drawn:

This approach for identifying given biological images was tested and in 97.5% of all cases, clouds of nipple points of the cow were formed.

Analyzing the work of the developed identification algorithm, it was noticed that the algorithm worked out too long, reaching up to 6 seconds. This is due to the fact that at the entrance to the developed algorithm a matrix with data of more than 90 thousand points arrives, which entails an increase in the processing time of the input information. To reduce operating space costs, it is recommended to reduce the number of points for analysis in those places where their number does not affect the content of the resulting point clouds.

Although the experimental results demonstrated the reliability of the presented approach, further testing is required to determine the ability of the system to cope with various scenarios existing in natural conditions.

7. References

[1] Weingarten J., Gruener G., and Siegwart R. (2004). A state-of-the-art 3D sensor for robot navigation, in Proc. IEEE/RSJ Int. Conf. Intell. RobotsSyst., vol. 3, Sendei, Sep. 2004, pp. 2155–2160. DOI: 10.1109/IROS.2004.1389728.

[2] Kowalski, M., Piszczek, M., Szustakowski, M., Ciurapinski, W. (2012). Single-pixel camera - simulation tool and the first results of analysis of image quality. Proceedings of the 23rd International DAAAM Symposium, Volume 23, No.1, pp. 309-312.

[3] Hussmann S. and Liepert T. (2007). Robot vision system based on a 3D-ToFcamera, in Proc. 24th IEEE Instrum. and Meas. Tech. Conf., vol. 1-5, Warsaw, May 2007, pp. 1405–1409. DOI: 10.1109/IMTC.2007.379356.

[4] Dellen B., Aleny`a G., Foix S., and Torras C. (2009). 3D object reconstruction from Swissranger sensors data using a spring-mass model, in Proc. 4thInt. Conf. Comput. Vision Theory and Applications, vol. 2, Lisbon, Feb.2009, pp. 368–372.

[5] Foix S., Aleny`a G., Andrade-Cetto J., and Torras C. (2010). Object modeling using a ToF camera under an uncertainty reduction approach, in Proc. IEEE Int. Conf. Robot. Automat., Anchorage, May 2010, pp. 1306–1312. DOI: 10.1109/ROBOT.2010.5509197.

[6] Liu X. and Fujimura K. (2004). Hand gesture recognition using depth data, in Proc. 6th IEEE Int. Conf. Automatic Face Gesture Recog., Seoul, May 2004, pp. 529–534. DOI: 10.1109/AFGR.2004.1301587.

[7] Gokturk S. B. and Tomasi C. (2004). 3D head tracking based on recognitionand interpolation using a time-of-flight depth sensor, in Proc. 18th IEEE Conf. Comput. Vision Pattern Recog., vol. 2, Washington DC, June-July 2004, pp. 211–217. DOI: 10.1109/CVPR.2004.1315166.
[8] Nanda K., Fujimura H. (2004). Visual tracking using depth data, in Proc. IEEE CVPR Workshops, vol. 3, Washington, D. C., June 2004, pp. 37–37. DOI: 10.1109/CVPR.2004.202.
[9] Paredes, J.A., Álvarez, F.J., Aguilera, T., Aranda, F.J. (2020). Precise drone location and tracking by adaptive matched filtering from a top-view, Expert Systems with Applications, Vol. 141, 1 March 2020. DOI: 10.1016/j.eswa.2019.112989.
[10] Bourhane Kadmiry, Chee Kit Wong, P.P.K. Lim. (2014). Vision-based approach for the localisation and manipulation of ground-based crop, International Journal of Computer Applications in Technology, January 2014, DOI: 10.1504/IJCAT.2014.063909.
[11] Choi, J.; Yin, X.; Yang, L.; Noguchi, N. (2014). Development of a laser scanner-based navigation system for a combine harvester. Eng. Agric. Environ. Food 2014, 7, 7–13
[12] IFM Electronic 3D Smart Sensor – Your Assistant on Mobile Machines. Available online: http://www.ifm.com (accessed on 22 January 2016).
[13] Nakarmi, A.; Tang, L. (2012). Automatic inter-plant spacing sensing at early growth stages using a 3D vision sensor. Comput. Electron. Agric. 2012, 82, 23–31.
[14] Gongal, A.; Amatya, S.; Karkee, M. (2014). Identification of repetitive apples for improved crop-load estimation with dual-side imaging. In Proceedings of the ASABE and CSBE/SCGAB Annual International Meeting, Montreal, QC, Canada, 13–16 July 2014; Volume 7004, pp. 1–9.
[15] Akhloufi M. A. (2014). 3D vision system for intelligent milking robot automation // The conference Intelligent Robots and Computers Vision XXXI: Algorithms and Techniques. 2014. Vol. 9025.
[16] Garrido, M.; Paraforos, D.S.; Reiser, D.; Arellano, M.V.; Griepentrog, H.W.; Valero, C. (2015). 3D Maize Plant Reconstruction Based on Georeferenced Overlapping LiDAR Point Clouds. Remote Sens. 2015, 7, 17077–17096.
[17] Underwood, J.; Calleija, M.; Nieto, J.; Sukkarieh, S. (2013). A robot amongst the herd: Remote detection and tracking of cows. In Proceedings of the 4th Australian and New Zealand spatially enabled livestock management symposium; Ingram, L., Cronin, G., Sutton, L., Eds.; The University of Sydney: Camden, Australia, 2013; p. 52.
[18] Dorokhov A., Kirsanov V., Pavkin D., Shilin D., Shestov D., Kuzin S. (2019). Calculation of the Manipulator's Kinematic Model and Mounting Points of the Drive Equipment. In Proc. 2nd International Conference on Intelligent Computing and Optimization, vol. 1072, Koh Samui, Thailand, Oct. 2019, pp. 339–348. DOI: 10.1007/978-3-030-33585-4_34.
[19] Ganin, P.E., Shilin, D.V., Shestov, D.A. (2019). Building Unified Control System for Multi-Link Industrial Manipulators, Proceedings - 2019 International Russian Automation Conference,September 2019, DOI: 10.1109/RUSAUTOCON.2019.8867705.
[20] Sappa A., Restrepo-Specht A. and Devy M. (2001). Range Image Registration by using an Edge–based Representation. In: Proceedings of the 9th International Symposium on Intelligent Robotic Systems, pp. 167-176. DOI: 10.1007/11848035_98.
[21] Rabbania T., van den Heuvelb F. A., Vosselmanc G. (2006). Segmentation of point clouds using smoothness constraint, Int. Arch. Photogramm. Remote Sens. Spat. Inform. Sci. 2006.
[22] Felsberg, Forssén, & Scharr. (2006). Channel Smoothing: Efficient Robust Smoothing of Low-Level Signal Features. IEEE Transactions on Pattern Analysis and Machine Intelligence, Vol. 28 , Issue: 2 , Feb. 2006, pp. 209-222, DOI: 10.1109/TPAMI.2006.29.
[23] Oytun Akman, Neslihan Bayramoglu, A. Aydın Alatan, Pieter Jonker. (2010). Utilization of spatial information for point cloud segmentation, Conference: 3DTV-Conference: The True Vision - Capture, Transmission and Display of 3D Video (3DTV-CON), 2010. DOI: 10.1109/3DTV.2010.5506339.
[24] Deckers, N., Reulke, R. (2019). Comparison of Three-Dimensional Scanning Devices. International Conference Image and Vision Computing New ZealandVolume, December 2019. DOI: 10.1109/IVCNZ48456.2019.8961017.
[25] Bogaerts Boris, Pernie Kadi, Sels Seppe, Ribbens Bart, Vanlanduit Steve. (2016).A simple evaluation procedure for range camera measurement quality, Conference: ACIVS, October 2016, Vol. LNCS 10016. DOI: 10.1007/978-3-319-48680-2_26
[26] Kolb, A., Barth, E., Koch, R. and Larsen, R. (2009). Time-offlight sensors in computer graphics, in Proc. Eurographics State of the Art Reports, pp.119–134.
[27] Min Dai, Timothy S. Newman, Chunguang Cao. (2008). Least-squares-based fitting of paraboloids. Pattern Recognition, 40, pp. 504-515. DeLaval. (2008). DOI:10.1016/j.patcog.2006.01.016.